Computers and Fluids 156 (2017) 1–8

Contents lists available at ScienceDirect

Computers and Fluids

journal homepage: www.elsevier.com/locate/compfluid

Benchmark solutions

A comparative study of boundary conditions for lattice Boltzmann simulations of high Reynolds number flows

Kainan Hu[a,b], Jianping Meng[c,*], Hongwu Zhang[a], Xiao-Jun Gu[c], David R Emerson[c], Yonghao Zhang[d]

[a] Industrial Gas Turbine Laboratory, Institute of Engineering Thermophysics, Chinese Academy of Sciences, Beijing, China
[b] University of Chinese Academy of Sciences, Beijing, China
[c] Scientific Computing Department, STFC Daresbury laboratory, Warrington WA4 4AD, United Kingdom
[d] James Weir Fluids Laboratory, Department of Mechanical & Aerospace Engineering, University of Strathclyde, Glasgow, G1 1XJ, UK

ARTICLE INFO

Article history:
Received 27 June 2016
Revised 7 June 2017
Accepted 13 June 2017
Available online 15 June 2017

Keywords:
Lattice Boltzmann method
Bounce-back scheme
Non-equilibrium bounce-back scheme
Non-equilibrium extrapolation scheme
Kinetic boundary condition
Cavity flow

ABSTRACT

Four commonly-used boundary conditions in lattice Boltzmann simulation, i.e. the bounce-back, non-equilibrium bounce-back, non-equilibrium extrapolation, and the kinetic boundary condition, have been systematically investigated to assess their accuracy, stability and efficiency in simulating high Reynolds number flows. For the classical lid-driven cavity flow problem, it is found that the bounce-back scheme does not influence the simulation accuracy in the bulk region if the boundary condition is properly implemented to avoid generating non-physical slip velocity. Although the kinetic boundary condition naturally produces physical slip velocity at the wall, it gives overall satisfactory predictions of the center-line velocity profile and the vortex center locations for the Reynolds numbers considered. For the cavity flow problem, all four boundary conditions show minimal difference in the computing time needed to reach a steady state. This is surprising because the kinetic boundary condition is significantly different from the other three schemes which are designed specifically for no-slip boundary conditions. The bounce-back scheme is the most computationally efficient in updating boundary points, which is particularly attractive if there are a large number of solid bodies in the flow field. For the numerical stability, we further test the pressure-driven channel flow with or without a enclosed square cylinder. Overall, the kinetic boundary condition is the most stable of the four schemes. The non-equilibrium extrapolation scheme presents excellent stability second to the kinetic boundary condition for the lid-driven cavity flow. In comparison with other threes schemes, the stability of non-equilibrium bounce-back scheme appears to be less satisfactory for both flows.

1. Introduction

The lattice Boltzmann (LB) method has been developed into an efficient mesoscopic simulation tool for fluid dynamics [1], which has shown its strength in simulating multi-phase and multi-component flows [2], and flows in porous media [3]. Its potential for simulating high Reynolds number (*Re*) flows has also attracted significant interest. For example, with a second-order numerical scheme in both time and space, the LB method was shown to perform well for decaying turbulence, although it may require higher spatial resolution, with a correspondingly smaller time step, in comparison to a spectral method [4]. However, a high-order LB model has been successfully applied for simulating the Kida vortex flow [5]. There have been various attempts to simulate turbulence including large eddy simulation and direct numerical simulation [6].

It is of importance to choose an appropriate boundary condition for simulating high-*Re* flows as it is often the key to stability, efficiency, and accuracy of simulations, particularly for complex geometry [7]. Conventionally, we need to implement the macroscopic no-slip boundary condition, which has many different implementations in the LB method because of its mesoscopic nature. The most commonly-used implementation is the bounce-back (BB) scheme, which originally describes a stationary wall. However, with a simple modification, it can be used for moving walls as well [8]. By assuming bounce-back of the non-equilibrium part of the distribution function, Zou and He derived the so-called non-equilibrium bounce-back (NEBB) boundary condition [9] for both moving and

* Corresponding author.
E-mail addresses: hukainan@iet.cn (K. Hu), jianping.meng@stfc.ac.uk, jpmeng@gmail.com (J. Meng), zhw@iet.cn (H. Zhang), xiaojun.gu@stfc.ac.uk (X.-J. Gu), david.emerson@stfc.ac.uk (D.R. Emerson), yonghao.zhang@strath.ac.uk (Y. Zhang).

http://dx.doi.org/10.1016/j.compfluid.2017.06.008

stationary walls. Guo et al. [10,11] proposed the non-equilibrium extrapolation (NEEP) scheme, which is also suitable for both moving and stationary walls. There are also other implementations, e.g., the counter-slip boundary [12].

The kinetic boundary condition (KBC) is of great interest for the LB method [13]. This scheme can induce physically realistic slip velocity at a wall boundary, and has been often used in the discrete velocity method (DVM) [14] for rarefied gas flows, e.g., [15]. As a special form of DVM, the LB method can also use the KBC to simulate rarefied gas flows over a broad range of Knudsen numbers (Kn) [16]. Moreover, the KBC has a nice property of retaining the positivity of outgoing particle distribution functions at the boundary nodes if the incoming mass flux is positive, which is helpful for numerical stability. Therefore, it is interesting to investigate its performance for high-Re flows.

The accuracy of the BB scheme has been studied in detail for simple flows, e.g. [17,18]. It was shown that the BB scheme may induce a numerical slip velocity and cause different order of errors depending on its implementation (e.g.,"on-grid" or "halfway"). While this artificial slip velocity can be eliminated for simple geometries [19], we will investigate the performance of the BB scheme without the deficiency.

Other boundary schemes are also assessed in the literature including those specifically designed for curved boundaries (see e.g., [20–22]). Of particular interest is that the NEEP scheme shows second-order accuracy for "moderate" Reynolds number flows in complex domains [20], which is consistent with the analysis in [10,11,18] for relatively simple flows. Moreover, the scheme also presents sufficient numerical stability for the investigated Reynolds numbers.

In this work, we will focus on accuracy, efficiency, and stability of the BB, NEEP NEBB and the KBC schemes for high Reynolds number flows. Our benchmark simulations will be conducted using a D2Q9 lattice model for the classical lid-driven cavity flow and the flow around a square cylinder confined in a channel. The results will be particularly focused on the cavity flow where we are able to assess the four boundary schemes for Reynolds numbers up to 7500. For the flow around a square cylinder, we will primarily investigate their numerical stability.

2. Lattice Boltzmann equation and D2Q9 lattice model

The LB method can be considered as an approximation to the Boltzmann-BGK equation [23–25]. The governing equation can be written as

$$\frac{\partial f_\alpha}{\partial t} + \boldsymbol{c}_\alpha \cdot \nabla f_\alpha = -\frac{1}{\tau}(f_\alpha - f_\alpha^{eq}). \tag{1}$$

This equation describes the evolution of the distribution $f_\alpha(\boldsymbol{x}, t)$ for the discrete velocity $\boldsymbol{c}_\alpha$ at position $\boldsymbol{x}$ and time t. The complex molecular interaction is simplified as a relaxation scheme towards the discrete equilibrium distribution $f_\alpha^{eq}(\boldsymbol{x}, t)$. In order to simulate incompressible and isothermal flows, it is common to use an equilibrium function with second-order velocity terms

$$f_\alpha^{eq} = w_\alpha \rho \left[1 + \frac{\boldsymbol{u}\cdot\boldsymbol{c}_\alpha}{RT_0} + \frac{1}{2}\frac{(\boldsymbol{u}\cdot\boldsymbol{c}_\alpha)^2}{(RT_0)^2} - \frac{\boldsymbol{u}\cdot\boldsymbol{u}}{2RT_0}\right], \tag{2}$$

which is determined by the density, ρ, the fluid velocity, $\boldsymbol{u}$,, and the reference temperature, T_0. For gas flows, the constant, R, can be conveniently understood as the gas constant. If a liquid is involved, R, together with T_0, can be considered as a reference quantity. For convenience, the sound speed c_s is often considered to be $\sqrt{RT_0}$, although there is a constant factor $\sqrt{\gamma}$ of difference where γ is the ratio of specific heats. The weighting factor is denoted by w_α for the discrete velocity $\boldsymbol{c}_\alpha$. Although the LB method appears to be a primary tool for modeling gas flow, based on its origin from kinetic theory, it can also be used for liquid flows. This utilizes the fact that, under appropriate conditions, the Navier–Stokes (NS) equations can be recovered, which is valid for both gas and liquid flows.

The relaxation time τ is related to the fluid viscosity via the Chapman–Enskog expansion, i.e., $\mu = p\tau$, where μ is the viscosity and p the pressure. Hence, for isothermal and incompressible flows, the Reynolds number becomes $Re = \rho_0 u_0 L/\mu = u_0 L/(\tau RT_0)$, where the subscript 0 denotes the reference value and L is the characteristic length of the system. It is worth noting that the important non-dimensional number, Kn, can be defined as $\mu_0\sqrt{RT_0}/(p_0 L)$. So, τ is also related to the Knudsen number through viscosity, i.e., $Kn = \tau\sqrt{RT_0}/L$ where $p_0 = \rho_0 RT_0$. We can therefore obtain $Kn \times Re = u_0/\sqrt{RT_0} = Ma$. For gas flows, the Knudsen number is the ratio of the gas mean free path and the characteristic length, which measures the rarefied level of gas flows. If a liquid flow is simulated, we may not be able to define a physically meaningful Knudsen number. However, the above defined Knudsen number can be regarded as an important "numerical" number for LB simulation due to its kinetic nature. In this case, this "numerical" Knudsen number will influence the dynamical behavior of modelling liquid flow. When Kn becomes large, the LB method may deviate from the NS dynamics significantly, even in the bulk region away from any surface [26]. Therefore, for liquid flows, it is important to ensure a small "numerical" Kn in any LB simulation in order to avoid deviating from the NS hydrodynamics. However, this is not a problem for gas flows. Instead, it provides an opportunity to model rarefied gas flows with suitable ranges of Knudsen numbers (see e.g. [16]).

For the isothermal case, only density and velocity are of interest and can be obtained as

$$\rho = \sum_\alpha f_\alpha, \text{ and } \rho\boldsymbol{u} = \sum_\alpha f_\alpha \boldsymbol{c}_\alpha. \tag{3}$$

A smart scheme can be utilized to numerically solve Eq. (1) and achieve the particle-jump like simulation [27]. By applying the trapezoidal integration rule for both sides of Eq. (1) and introducing a transformation

$$\tilde{f}_\alpha = f_\alpha + \frac{dt}{2\tau}(f_\alpha - f_\alpha^{eq}), \tag{4}$$

we obtain the discretized form for $\tilde{f}$ as

$$\tilde{f}_\alpha(\boldsymbol{x}+\boldsymbol{c}_\alpha dt, t+dt) - \tilde{f}_\alpha(\boldsymbol{x}, t) = -\frac{dt}{\tau + 0.5dt}\left[\tilde{f}_\alpha(\boldsymbol{x}, t) - f_\alpha^{eq}(\boldsymbol{x}, t)\right], \tag{5}$$

which provides the stream-collision algorithm.

The last key step is to choose an appropriate set of discrete velocities. The D2Q9 lattice is the most popular choice for two-dimensional flows, which employs nine discrete velocities

$$\boldsymbol{c}_\alpha = \begin{cases} (0,0), & \alpha = 0, \\ (\cos(\alpha-1)\pi/2,\ \sin(\alpha-1)\pi/2)\sqrt{3RT_0}, & \alpha = 1,2,3,4, \\ (\cos(2\alpha-9)\pi/4,\ \sin(2\alpha-9)\pi/4)\sqrt{3RT_0}, & \alpha = 5,6,7,8. \end{cases} \tag{6}$$

The corresponding weights are $w_0 = 4/9$, $w_{1-4} = 1/9$, $w_{5-8} = 1/36$.

As discussed, the stream-collision algorithm can readily be implemented now and the only requirement is to tie the space and time step together. If one is determined, the other is determined also. For instance, assuming the system length is L, we may set the space step dx and dy as $dx = dy = L/100$ and then $dt = L/(100\sqrt{3RT_0})$ with 100 cells of spatial resolution. This insures the "particles" are jumping on a uniform grid system. Alternatively,

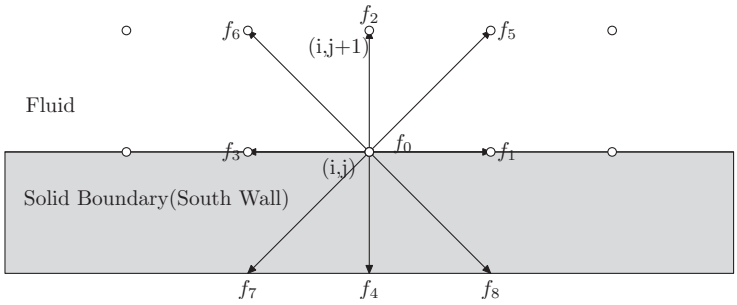

Fig. 1. Illustration of south (bottom) wall boundary.

Table 1
Parameters for two grids of a physical system defined by u_0, ν_0 and T_0, where $dx_0 = L/N$ is the spatial step size with N cells.

cell number	$dx(dt\sqrt{3RT_0})$	$\hat{u}_0$	$\hat{\tau}$	$\hat{\nu}$	$\hat{\tau}^o$
N	dx_0	$\frac{u_0}{\sqrt{3RT_0}}$	$\frac{3\nu_0}{dx_0\sqrt{3RT_0}}$	$\frac{\nu_0}{dx_0\sqrt{3RT_0}}$	$\frac{3\nu_0}{dx_0\sqrt{3RT_0}} + \frac{1}{2}$
$2N$	$\frac{dx_0}{2}$	$\frac{u_0}{\sqrt{3RT_0}}$	$\frac{6\nu_0}{dx_0\sqrt{3RT_0}}$	$\frac{2\nu_0}{dx_0\sqrt{3RT_0}}$	$\frac{6\nu_0}{dx_0\sqrt{3RT_0}} + \frac{1}{2}$

we may transform Eq. (1) to its non-dimensional form first and then apply the scheme given by Eq. (5), as done in [26]. Obviously, the non-dimensional transformation will not alter the final simulation results.

It is common to choose the space step dx or dy and time step dt as reference values, i.e., the "lattice" unit. For the D2Q9 model, the transformation is

$$\hat{\boldsymbol{x}} = \frac{\boldsymbol{x}}{dx}, \quad \hat{t} = \frac{t}{dt}, \quad \hat{\boldsymbol{u}} = \frac{\boldsymbol{u}}{\sqrt{3RT_0}}, \quad \hat{\boldsymbol{c}}_\alpha = \frac{\boldsymbol{c}_\alpha}{\sqrt{3RT_0}}, \quad \hat{\tau} = \frac{\tau}{dt}, \tag{7}$$

where the hat symbol is used to denote normalized variables in the lattice unit. Also, we note $dx = dt\sqrt{3RT_0}$. With the transformation, Eq. (5) becomes

$$\tilde{f}_\alpha(\hat{\boldsymbol{x}} + \hat{\boldsymbol{c}}_\alpha, \hat{t} + 1) - \tilde{f}_\alpha(\hat{\boldsymbol{x}}, \hat{t}) = -\frac{1}{\hat{\tau} + 0.5}\left[\tilde{f}_\alpha(\hat{\boldsymbol{x}}, \hat{t}) - f_\alpha^{eq}(\hat{\boldsymbol{x}}, \hat{t})\right]. \tag{8}$$

For convenience, a new relaxation time $\hat{\tau}^o = \hat{\tau} + 0.5$ is always introduced. In addition, it is also common practice to calculate the important non-dimensional variables in the lattice unit, i.e.,

$$Re = \frac{u_0 L}{\nu} = \frac{\hat{u}_0 \hat{L}}{\hat{\nu}}, \quad Kn = \frac{\tau\sqrt{RT_0}}{L} = \frac{\hat{\tau}}{\hat{L}\sqrt{3}}, \tag{9}$$

where ν denotes the kinematic viscosity and we have $\nu = \hat{\nu} dx\sqrt{3RT_0}$. The length $\hat{L}$ in the lattice unit becomes the cell number of one coordinate and is commonly denoted as N. Finally, the relation between the viscosity and relaxation time in the lattice unit is

$$RT_0\tau = \nu \Rightarrow \frac{\hat{\tau}}{3} = \hat{\nu} \Rightarrow \frac{\hat{\tau}^o - 0.5}{3} = \hat{\nu}. \tag{10}$$

While any proper transformations will not influence the final results, we find that an issue may occur with the lattice unit when conducting grid independent tests. For convenience, we consider isothermal and incompressible flow. Following the aforementioned procedure, we list parameters in both the physical unit and lattice unit of two different grid systems in Table 1. The physical system is defined by a set of fixed parameters u_0, ν_0 and T_0. It shows that, to keep all the parameters exactly the same in physical units, the relaxation time and viscosity in the lattice unit should depend linearly on the mesh size. It is different from the practice where the viscosity $\hat{\nu}$ in the lattice unit is fixed. From the above transformation and Table 1, if $\hat{\nu}$ and Re are fixed, the corresponding physical system needs to have either a different viscosity or a different characteristic length while the characteristic velocity must be changed. This turns out to be, however, inconsistent with common CFD practice. In fact, since both Ma and Kn are changed in this way, there is a risk that Kn for the coarsest mesh becomes so large (cf. Eq. 9) that the LB method may deviate from the NS dynamics, even in the bulk [26]. For this reason, we shall keep all the parameters unchanged in physical units for grid independent tests or scheme accuracy analysis.

3. Numerical assessment of various boundary conditions

3.1. Boundary conditions

We choose to discuss the KBC and the BB, NEBB, NEEP schemes, and their implementation is illustrated in Fig. 1. For any boundary scheme, the aim is to determine the outgoing distribution functions f_5^b, f_2^b and f_6^b, where the superscript b is used to denote boundary point, according to the incoming distribution functions f_7^b, f_4^b and f_8^b known from the stream step. It is worth noting that we will use the "on-grid" implementation for all four boundary conditions.

The main idea of the BB scheme is that an incoming particle distribution directing to the wall bounces back into the fluid domain in the opposite direction. Therefore, for the D2Q9 model, we have $f_5^b = f_7^b$, $f_2^b = f_4^b$ and $f_6^b = f_8^b$. As discussed in [19], the non-physical slip velocity can be easily eliminated for this cavity flow by taking care of f_1^b and f_3^b.

The KBC assumes that an outgoing particle completely forgets its history and its velocity is renormalized by the Maxwellian distribution. Its implementation for the LB method has been discussed not only for standard models [13] but also for multi-speed models [28]. For the D2Q9 model as shown in Fig. 1, the rule can be simplified as,

$$f_\alpha^b = \frac{f_4^b + f_7^b + f_8^b}{f_2^{eq}(\rho_w, \boldsymbol{u}_w) + f_5^{eq}(\rho_w, \boldsymbol{u}_w) + f_6^{eq}(\rho_w, \boldsymbol{u}_w)} \times f_\alpha^{eq}(\rho_w, \boldsymbol{u}_w), \quad \alpha = 2, 5, 6, \tag{11}$$

where the wall density ρ_w is determined according to mass conversation and is actually canceled in the above formula.

In the NEBB scheme [9], the unknown distribution functions are solved by setting the constraints of

$$\sum_\alpha f_\alpha = \rho_w, \quad \sum_\alpha c_\alpha f_\alpha = \rho_w \boldsymbol{u}_w. \tag{12}$$

The equations are indefinite since there are more unknowns than equations. To resolve this, the distribution is first divided into the equilibrium and non-equilibrium parts and the bounce-back scheme is assumed to be valid for the non-equibrilium part of distribution function normal to the wall, i.e.,

$$f_2^b - f_2^{eq,b} = f_4^b - f_4^{eq,b}. \tag{13}$$

With this assumption, all unknown distribution functions can be determined.

The last boundary condition is the non-equilibrium extrapolation scheme [10,11,29], which divides all the unknown boundary distribution functions into two parts: the equilibrium part $f_\alpha^{eq,b}$ and the non-equilibrium part $f_\alpha^{neq,b}$,

$$f_\alpha^b = f_\alpha^{eq,b} + f_\alpha^{neq,b}. \tag{14}$$

For the D2Q9 model, the equilibrium part is

$$f_\alpha^{eq,b} = f_\alpha^{eq}(\rho^1, \boldsymbol{u}_w), \ \alpha = 2, 5, 6, \tag{15}$$

The non-equilibrium part is approximated as

$$f_\alpha^{neq,b} = f_\alpha^1 - f_\alpha^{eq,1}[\rho^1, \boldsymbol{u}^1], \ \alpha = 2, 5, 6, \tag{16}$$

where ρ^1 and $\boldsymbol{u}^1$ denote the quantities at the node $(i, 1)$, as shown in Fig. 1. Obviously, a first-order extrapolation scheme is used for both the density and the non-equilibrium part. However, it has been shown that the NEEP scheme can give second-order accuracy for incompressible flows [11].

3.2. Accuracy, stability and efficiency for lid-driven cavity flow

In the following we will compare accuracy, numerical stability and efficiency of these four schemes for simulating the classical lid-driven cavity flow problem. The fluid is confined in a square box but the top (north) lid of the box is moving with a constant speed. The Reynolds number and the top wall speed (i.e., Ma) will be specified for each of the following simulation. We will mainly consider steady flows with Re smaller than 7500, so that we can focus on the effect of boundary conditions without interference of physical instability. Hence, the criterion

$$E = \frac{\sqrt{\sum_{i,j}[u_x(i,j,t+dt)-u_x(i,j,t)]^2+[u_y(i,j,t+dt)-u_y(i,j,t)]^2}}{\sqrt{\sum_{i,j}[u_x(i,j,t+dt)^2+u_y(i,j,t+dt)^2]}} \tag{17}$$

is used to judge whether the steady state is reached, where u_x and u_y are the x-component and y-component of the velocity, $\boldsymbol{u}$, respectively. In our simulations, the largest value of E is 10^{-6}.

For a no-slip boundary condition, we need first to ensure no-slip can be correctly achieved. For example, we need to eliminate any non-physical slip velocity at a boundary for the BB scheme [19]. Therefore, accuracy analysis for a scheme can focus on numerical error related to mesh size in a common convergence test.

It is found that predictions for all boundary schemes are close to the benchmark results, given the fact that the KBC will produce slip velocity at a wall boundary, see Fig. 2 for the velocity profiles through centerlines and Table 2 for predictions of the vortex center location. This confirms, as expected, that the KBC can be used for flows with very low Knudsen and high Reynolds numbers. In fact, Fig. 3 shows decreasing velocity slip with increasing Re (and decreasing Kn) while Ma is fixed, which indicates that the impact of the slip velocity caused by KBC will become negligible for high Reynolds numbers and supports the findings in Fig. 2 and Table 2. It is also worthwhile to note that the slip velocity produced by the KBC represents physical effects for gas flows. The BB boundary scheme also works well since the non-physical slip is removed here.

We now perform common convergence tests for accuracy analysis. Following the discussion in Section 2, we keep all parameters unchanged in physical units. We check the results at a series of centerline points adjacent to the wall boundary, namely $x = 0.5$ and $y = 1/32, 1/16, 1/8, 1/4$. A moderate Reynolds number of 400 is considered and the top wall speed is set to be 0.1 in the lattice unit. Five sets of grids are investigated for each boundary condition, namely 96 × 96, 128 × 128, 192 × 192, 256 × 256 and 512 × 512. The results with the finest grid are considered to be "correct" to calculate the actual simulation accuracy, which is shown in Fig. 4.

All the simulations show similar accuracy, although those using the NEEP scheme show slightly higher accuracy. It is interesting to see that the simulations with the BB scheme can achieve accuracy better than first-order. This reflects the fact that the convergence test is actually measuring the accuracy of second order of Eq. (5) (cf. Ref. [17], particularly Eq. (10) in Page 121.) once the non-physical slip is carefully removed for the BB scheme, even with an on-grid implementation. Moreover, in comparison with the other three schemes, the first-order extrapolation of the NEEP scheme appears to enhance the simulation accuracy in the bulk region.

To study the numerical stability, we carry out two different tests. For the first test, we use a fixed number of grid points to simulate different Reynolds number, and record the maximum Re that can be achieved stably; For the second, the Reynolds number is fixed with a difference number of grid points for the simulations. We then record the minimum grid point number needed for a stable simulation. The results are listed in Tables 3 and 4. The KBC shows excellent stability, which can be attributed to the favorable property of positivity. The NEEP scheme also has good stability while the NEBB scheme is the less satisfactory.

The numerical efficiency of the boundary conditions is also measured by two criteria: the computational time needed for approaching the steady state determined by setting $E = 10^{-6}$ in Eq. (17) and the computational time for updating the wall boundary points. For this purpose, we run simulations on an Intel Core i5 3.20GHZ CPU. The results for the first criterion are listed in Table 5. There is no significant difference between the four schemes. This is particularly interesting for the KBC because previous simulations, using a discrete velocity model, became increasingly slower as the Knudsen number decreased [15] for rarefied gas flows. If we consider the lattice Boltzmann model to be a special form of the discrete velocity model, the evidence here shows that it presents little difference to those specially designed boundary conditions for continuum flows.

In Table 6, we list the computational time for updating all boundary points at the four walls during one time step. It is found that the NEEP boundary condition needs the longest time, which is around 40 times more expensive than the most efficient BB scheme. This shows that the BB scheme should be an efficient choice for simulating flows with a large percentage of solid boundary points, such as particle-fluid multiphase flows.

3.3. Stability for flow around a square cylinder

A two-dimensional channel flow around a square cylinder is utilized here to further assess the numerical stability of the four boundary schemes. The channel length and height is set to be L and H, respectively. The square is of width D and its center is located at the point $(4.5D, H/2)$. For convenience, we choose the channel height H as the reference length to define the Reynolds number as well as the Knudsen number. The flow is driven by the pressure difference between the inlet and outlet of the channel. The pressure profiles at the inlet and outlet are specified using a first-order extrapolation scheme which is implemented in the way described in, e.g., [32]. While both the NEEP scheme and the NEBB scheme can be used as the pressure flow boundary, they will not be employed in our comparisons to avoid the unnecessary coupling effect. Also, to eliminate the impact of transient effects on the comparison, steady cases will be considered here so that the Reynolds number will not be as high as those in the lid-driven cavity flows. However, to make the stability tests sensible, we will

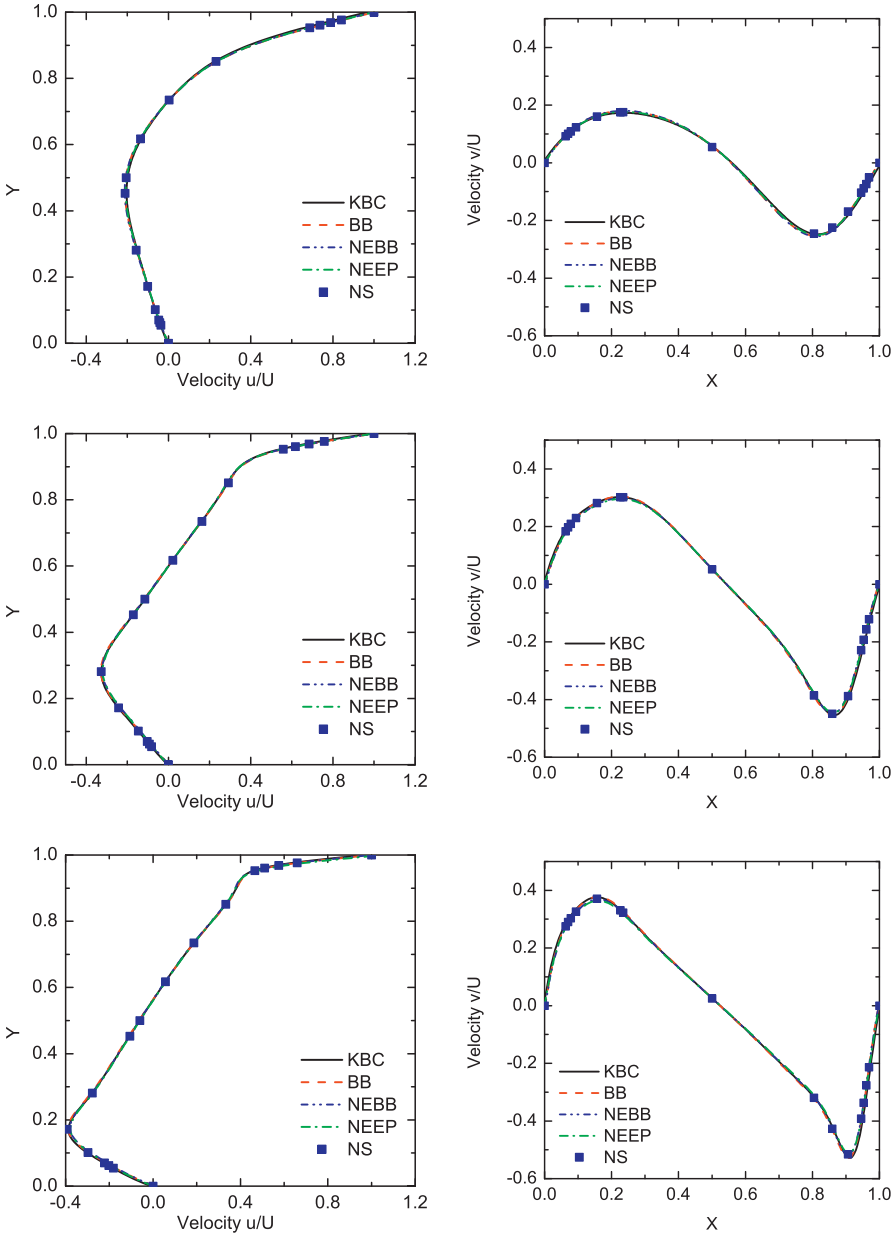

Fig. 2. Profiles of horizontal (vertical) velocity component through the vertical (horizontal) centerline of cavity at $Re = 100$ (top), $Re = 400$ (middle) and $Re = 1000$ (bottom). The horizontal and vertical components, $\hat{u}$ and $\hat{v}$, are normalized by the lid speed $\hat{U}$, which is set to be 0.1 for all three cases. The 'NS' solutions are taken from Ghia et al. [30].

carefully setup flows so that critical $\hat{\tau}^o$ values in the lattice unit can be achieved, i.e., approaching 0.5.

As with prior tests, we start from a pressure-driven flow without the enclosed square cylinder. The pressure difference is set to be the 0.00005 ($\times\ \rho_0 RT_0$) and the ratio L/D is set to be 100. For this geometry, we test two sets of Reynolds numbers (calculated based the maximum speed at the centerline), 0.0216 and 2.16, and the corresponding Knudsen numbers are 0.0017 and 0.00017. With these parameters, the relaxation time $\hat{\tau}^o$ in the lattice unit could be fairly small and approach critical value for stability if the mesh is coarse. For instance, using 500 × 5 cells, $\hat{\tau}^o$ is 0.5147 and 0.5015 receptively, see Eqs. (9) and (10) for the conversion. We then test the stability of four wall boundary schemes by varying mesh size. It is found that the KBC and the BB scheme allow stable simulations by using 500 × 5 cells for both Reynolds numbers, which demonstrate nice stability. For the NEEP scheme, 4000 × 40 cells ($\hat{\tau}^o = 0.618$) are required for a stable simulation with $Re = 0.0216$ while the correct solution is obtained. For $Re = 2.16$, we cannot obtain a stable simulation with up to 20000 × 200 cells ($\hat{\tau}^o = 0.559$). This observation is generally consistent with previous findings. In [11], it is found that $\hat{\tau}^o \approx 0.51$ is the threshold if the pressure inlet/outlet is also implemented using the NEEP scheme, while the critical value becomes approximately 0.7 if extrapolation schemes are used for both wall and flow boundary. Therefore, the less satisfactory stability behavior of the NEEP scheme may be attributed to the mixing with the extrapolation pressure flow boundary. We also note that the NEEP scheme appears to work well with a fixed velocity inlet boundary condition for similar flow problems [20]. The NEBB scheme also fails to achieve a stable simulation with 20000 × 200 cells for $Re = 2.16$.

Table 2
Comparison of vortex center locations. In all the present simulations, the top (north) wall speed is 0.1 in lattice units. The benchmark results by Hou et al. are taken from the LB solutions listed in Table I of [31] and those of Ghia et al. are from [30]. Using the grid 256 × 256, the NEBB scheme fails to maintain stable simulations for $Re = 5000$.

Re	Scheme/Source	Grid	Primary Vortex		Lower left vortex		Lower right vortex	
			x	y	x	y	x	y
400	KBC	256 × 256	0.5568	0.6084	0.0498	0.0481	0.8848	0.1237
	NEBB	256 × 256	0.5574	0.6062	0.0478	0.0476	0.8865	0.1219
	NEEP	256 × 256	0.5579	0.6076	0.0462	0.0470	0.8854	0.1223
	BB	256 × 256	0.5575	0.6067	0.0477	0.0468	0.8859	0.1217
	Hou et al.	256 × 256	0.5608	0.6078	0.0549	0.0510	0.8902	0.1255
	Ghia et al.		0.5547	0.6055	0.0508	0.0469	0.8906	0.1250
1000	KBC	256 × 256	0.5321	0.5635	0.0835	0.0775	0.8636	0.1145
	NEBB	256 × 256	0.5323	0.5657	0.0826	0.0759	0.8652	0.1122
	NEEP	256 × 256	0.5328	0.5672	0.0808	0.0753	0.8642	0.1132
	BB	256 × 256	0.5324	0.5659	0.0815	0.0709	0.8648	0.1130
	Hou et al.	256 × 256	0.5333	0.5647	0.0902	0.0784	0.8667	0.1137
	Ghia et al.		0.5313	0.5625	0.0859	0.0781	0.8594	0.1094
2000	KBC	256 × 256	0.5241	0.5468	0.0851	0.1002	0.8487	0.0957
	NEBB	512 × 512	0.5242	0.5474	0.0863	0.1013	0.8473	0.0976
	NEEP	256 × 256	0.5229	0.5485	0.0863	0.1011	0.8451	0.0977
	BB	256 × 256	0.5232	0.5475	0.0863	0.1016	0.8460	0.0976
	Hou et al.	256 × 256	0.5255	0.5490	0.0902	0.1059	0.8471	0.0980
5000	KBC	256 × 256	0.5150	0.5313	0.0729	0.1368	0.8044	0.0727
	NEBB	256 × 256	––	––	––	––	––	––
	NEEP	256 × 256	0.5156	0.5357	0.0742	0.1337	0.8052	0.0746
	BB	512 × 512	0.5167	0.5331	0.0743	0.1334	0.8092	0.0736
	Hou et al.	256 × 256	0.5176	0.5373	0.0784	0.1373	0.8078	0.0745
	Ghia et al.		0.5117	0.5352	0.0703	0.1367	0.8086	0.0742

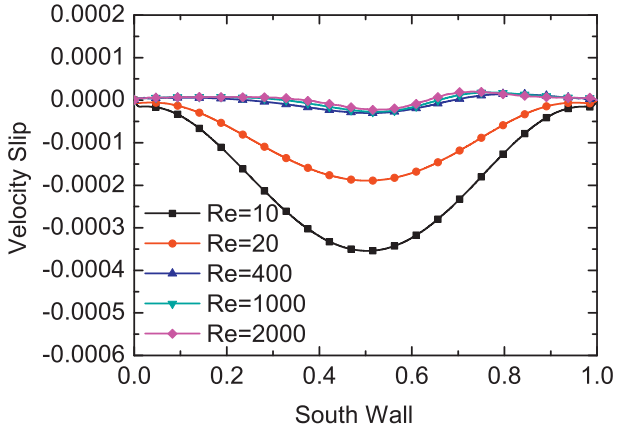

Fig. 3. Slip velocity induced by the KBC at the south (bottom) wall with different Reynolds numbers. The top wall speed is fixed to be 0.1 in lattice units so that *Re* is inversely proportional to *Kn* since $Kn \times Re = Ma$. The slip velocity is defined as the difference between the boundary horizontal velocity gained by computation and that of the stationary wall.

Table 3
Maximum Reynolds number achieved stably using a fixed number of grid points. For the KBC, the *Re* for 512 × 512 is not tested since the maximum *Re* is around 7500 for laminar flow.

Grid	KBC	NEBB	NEEP	BB
128 × 128	3000	400	1000	1000
256 × 256	7500	1000	5000	2000
512 × 512	––	2000	7500	5000

Table 4
Minimum number of grid points needed for simulating a fixed Reynolds number stably. For the case of $Re = 7500$, only a few thousand time steps are tested for the BB and NEBB schemes due to the large number of grid points.

Re	KBC	NEBB	NEEP	BB
1000	96 × 96	256 × 256	96 × 96	96 × 96
2000	128 × 256	512 × 512	256 × 256	256 × 256
7500	256 × 256	2048 × 2048	512 × 512	2048 × 2048

Table 5
Computational time (h) needed for approaching the steady state determined by setting the criterion, $E = 10^{-6}$, given by Eq. (17). The NEBB scheme is not tested for $Re = 5000$ since the simulation is not stable.

Re	Grid	KBC	NEBB	NEEP	BB
400	128 × 128	0.1038	0.1016	0.1010	0.1026
1000	256 × 256	1.2022	1.1025	1.3522	1.3540
2000	512 × 512	10.5536	10.2698	10.0537	10.3138
5000	512 × 512	33.0250	––	33.5905	32.8989

Table 6
Computational time (10^{-6} s) for updating boundary points.

Re	Grid	KBC	NEBB	NEEP	BB
1000	256 × 256	174	13.9	328	8.06

For the flow around a square cylinder, we will mainly investigate the stability of the KBC and the BB scheme based on the observation of the pressure-driven flow. For this purpose, the channel length L is set to be $15D$ and the height H equal to $2.5D$ where the flow will feel the blockage effects. To test the stability, we setup a case with 300 × 50 cells and $\hat{\tau}^o = 0.500866$ ($Kn = 0.00001$). The pressure difference is set to be 10^{-8} ($\times \rho_0 RT_0$). Both schemes can achieve a stable simulation, where "stable" means the simulation lasts at least 60000 iterations without the occurrence of "NAN" and afterwards we stop monitoring. This observation further verifies the stability of both the KBC and the BB scheme.

To examine the impact of the slip velocity, we set the pressure to be 1.0002 ($\times \rho_0 RT_0$) at the inlet and 1 ($\times \rho_0 RT_0$) at the outlet. If using 900 × 150 cells, it is found that the LB simulations with both boundary schemes are able to capture the vortices behind the square at a Knudsen number 0.00017 ($\hat{\tau}^o = 0.544$), as shown in

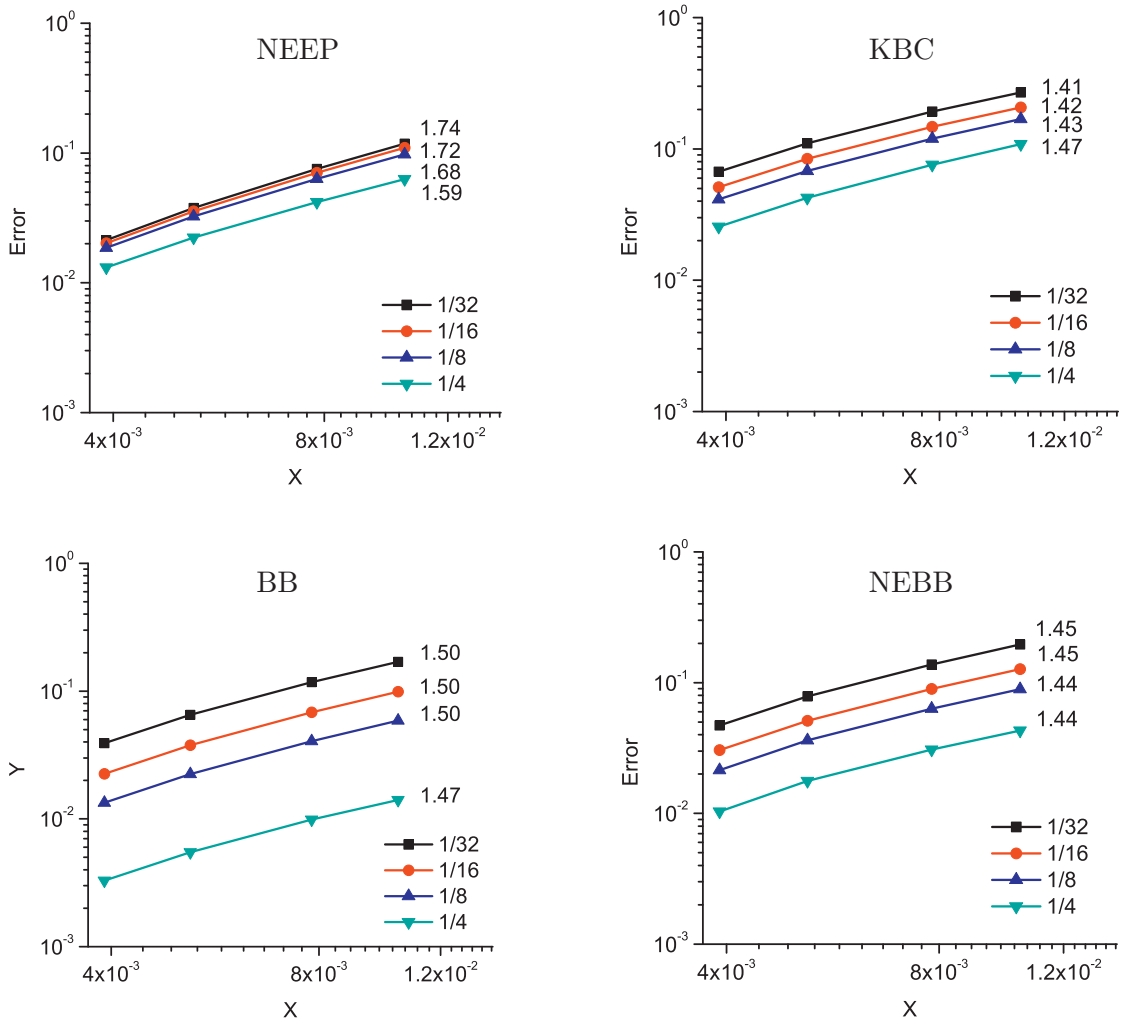

Fig. 4. Comparison of numerical accuracy relative to the numerical solution using 512 × 512 grid points at different points with boundary conditions KBC, BB, NEBB and NEEP. The accuracy order (slope) is shown by the figure beside each line. The Reynolds number is set to be 400 and the top wall speed 0.1 for all calculations.

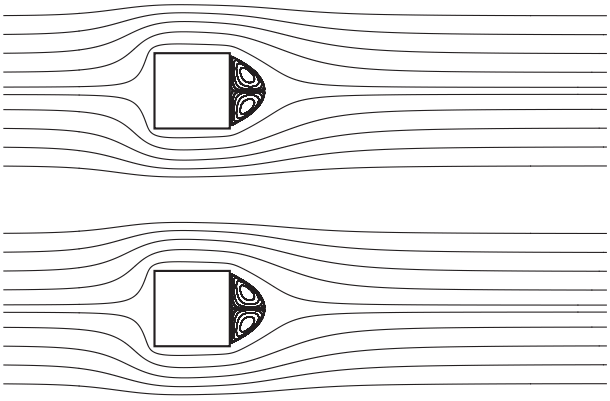

Fig. 5. Streamlines of the flow around a square cylinder captured by simulations using the BB scheme (top) and KBC (bottom). The Reynolds number is estimated to be 28 (see Section 3.3 for detail configuration).

Fig. 5. The Reynolds number is estimated to be about 28 using the average speed at the inlet. The simulation with the KBC produces qualitatively similar results to the one with the BB scheme, which again indicates that the slip velocity will play a minor role if the Knudsen number is small and the Reynolds number is sufficient large.

4. Concluding remarks

We have investigated the accuracy, stability, and efficiency of four popular boundary conditions for LB simulation of flows with high Reynolds numbers. For the present study, the classical lid-driven cavity problem is the primary benchmark application while the channel flow around a square cylinder is used to supplement the observation of numerical stability.

It is found that all four schemes give reasonable predictions of the centerline velocity profile and the vortex position for the lid-driven cavity flow. In particular, the slip velocity given by the KBC has no significant effect on the Reynolds numbers considered (low Knudsen number). Once the non-physical slip is removed, the BB boundary condition also performs well. Moreover, the discretization accuracy is not influenced by the BB scheme in the bulk region. In fact, simulations using any of the four boundary conditions give similar orders of accuracy for the tested bulk points. The KBC shows the best stability for not only the cavity flow but also the flow around a confined square cylinder, possibly because it is able to maintain its positivity of distribution function. The NEEP scheme shows excellent stability for the cavity flow. The BB scheme shows consistent stability behavior for both flows. In the present study,

we find that the computational time required to reach the steady state for the lid-driven cavity flow is similar for all four boundary conditions considered. Interestingly, the KBC scheme, which is often used for rarefied gas flows, shows no significant difference in comparison to the other three boundary conditions specially designed for continuum flows. However, both the KBC and NEEP schemes need a significantly longer time to update the boundary points while the BB boundary condition, as expected, is the most computationally efficient.

Acknowledgments

KNH and HWZ would like to thank the support of the National Key Research and Development Program of China under Grant No 2016YFB0200901. JPM and DRE would like to thank the Engineering and Physical Science Research Council (EPSRC) for their support under projects EP/L00030X/1, EP/N033841/1, EP/K038451/1 and EP/N016602/1. All authors from DL thanks by the Hartree center for their support. YHZ would like to thank the support of EPSRC under grant number EP/M021475/1.

References

[1] Chen S, Doolen GD. Lattice Boltzmann method for fluid flows. Annu Rev Fluid Mech 1998;30(1):329–64.
[2] Shan X, Chen H. Simulation of nonideal gases and liquid-gas phase transitions by the lattice Boltzmann equation. Phys Rev E 1994;49(4):2941.
[3] Wang M, Wang J, Pan N, Chen S. Mesoscopic predictions of the effective thermal conductivity for microscale random porous media. Phys Rev E 2007;75(3):036702.
[4] Peng Y, Liao W, Luo L-S, Wang L-P. Comparison of the lattice Boltzmann and pseudo-spectral methods for decaying turbulence: low-order statistics. Comput Fluids 2010;39(4):568–91.
[5] Chikatamarla SS, Frouzakis CE, Karlin IV, Tomboulides AG, Boulouchos KB. Lattice Boltzmann method for direct numerical simulation of turbulent flows. J Fluid Mech 2010;656:298–308.
[6] Aidun CK, Clausen JR. Lattice-Boltzmann method for complex flows. Ann Rev Fluid Mech 2010;42(1):439–72.
[7] Jahanshaloo L, Sidik NAC, Fazeli A, A MPH. An overview of boundary implementation in lattice Boltzmann method for computational heat and mass transfer. Int Commun Heat Mass 2016;78:1–12.
[8] Ladd AJC. Numerical simulations of particulate suspensions via a discretized Boltzmann equation. Part 1. Theoretical foundation. J Fluid Mech 1994;271:285–309.
[9] Zou Q, He X. On pressure and velocity boundary conditions for the lattice boltzmann BGK model. Phys Fluids 1997;9(6):1591–8.
[10] Guo ZL, Zheng CG, Shi BC. An extrapolation method for boundary conditions in lattice Boltzmann method. Phys Fluids 2002a;14(6):2007–10.
[11] Guo ZL, Zheng CG, Shi BC. Non-equilibrium extrapolation method for velocity and pressure boundary conditions in the lattice Boltzmann method. Chin Phys 2002b;11(4):366–74.
[12] Inamuro T, Yoshino M, Ogino F. A nonâslip boundary condition for lattice Boltzmann simulations. Phys Fluids 1995;7(12):2928.
[13] Ansumali S, Karlin IV. Kinetic boundary conditions in the lattice Boltzmann method. Phys Rev E 2002;66:026311.
[14] Gatignol R. Kinetic theory boundary conditions for discrete velocity gases. Phys Fluids 1977;20(12):2022–30.
[15] Valougeorgis D, Naris S. Acceleration schemes of the discrete velocity method: gaseous flows in rectangular microchannels. J Sci Comput 2003;25(2):534–52.
[16] Meng J, Zhang Y, Hadjiconstantinou NG, Radtke GA, Shan X. Lattice ellipsoidal statistical BGK model for thermal non-equilibrium flows. J Fluid Mech 2013;718:347–70.
[17] He X, Zou Q, Luo L-S, Dembo M. Analytic solutions of simple flows and analysis of nonslip boundary conditions for the lattice Boltzmann BGK model. J Stat Phys 1997;87:115–36.
[18] Suh YK, Kang J, Kang S. Assessment of algorithms for the no-slip boundary condition in the lattice Boltzmann equation of BGK model. Int J Numer Methods Fluids 2008;58(12):1353–78.
[19] Meng JP, Gu XJ, Emerson DR. Slip velocity of lattice Boltzmann simulation using bounce-back boundary scheme. ArXiv e-prints.
[20] Nash RW, Carver HB, Bernabeu MO, Hetherington J, Groen D, Krüger T, et al. Choice of boundary condition for lattice-Boltzmann simulation of moderate-Reynolds-number flow in complex domains. Phys Rev E 2014;89:023303.
[21] Latt J, Chopard B, Malaspinas O, Deville M, Michler A. Straight velocity boundaries in the lattice Boltzmann method. Phys Rev E 2008;77(5):56703.
[22] Kao P-H, Yang R-J. An investigation into curved and moving boundary treatments in the lattice boltzmann method. J Comput Phys 2008;227(11):5671–90.
[23] Shan XW, Yuan XF, Chen HD. Kinetic theory representation of hydrodynamics: a way beyond the Navier Stokes equation. J Fluid Mech 2006;550:413–41.
[24] Shan X, He X. Discretization of the velocity space in the solution of the Boltzmann equation. Phys Rev Lett 1998;80:65–8.
[25] He X, Luo L-S. Theory of the lattice Boltzmann method: from the Boltzmann equation to the lattice Boltzmann equation. Phys Rev E 1997;56:6811–17.
[26] Meng J, Zhang Y. Accuracy analysis of high-order lattice Boltzmann models for rarefied gas flows. J Comput Phys 2011;230(3):835–49.
[27] He X, Chen S, Doolen GD. A novel thermal model for the lattice Boltzmann method in incompressible limit. J Comput Phys 1998;146(1):282–300.
[28] Meng J, Zhang Y. Diffuse reflection boundary condition for high-order lattice Boltzmann models with streaming-collision mechanism. J Comput Phys 2014;258(0):601–12.
[29] Guo Z, Shu C. Lattice Boltzmann method and its applications in engineering. vol. 3 advances in computational fluid dynamicsWorld Scientific; 2013.
[30] Ghia U, Ghia KN, Shin C. High-re solutions for incompressible flow using the Navier–Stokes equations and a multigrid method. J Comput Phys 1982;48(3):387–411.
[31] Hou S, Zou Q, Chen S, Doolen G, Cogley AC. Simulation of cavity flow by the lattice Boltzmann method. J Comput Phys 1995;118(2):329–47.
[32] Verhaeghe F, Luo L-S, Blanpain B. Lattice Boltzmann modeling of microchannel flow in slip flow regime. J Comput Phys 2009;228(1):147–57.